A Platinum Open Access Journal for Organic Chemistry

Paper

Free to Authors and Readers

DOAJ Seal

Arkivoc **2022**, part ii, 0-0

to be inserted by editorial office

Synthesis and biochemical evaluation of 5-(pyridin-4-yl)-3-(alkylsulfanyl)-4*H*-1,2,4-triazol-4-amine-based inhibitors of tyrosinase from *Agaricus bisporus*

Laura De Luca,[a] Salvatore Mirabile,[a,b] Federico Ricci,[a] Ilenia Adornato,[a] Anna Cacciola,[a,b] Maria Paola Germanò [a] Rosaria Gitto[a,*]

[a]*CHIBIOFARAM Department, University of Messina, Viale Stagno D'Alcontres 31, I-98166, Messina, Italy*
[b]*Foundation Prof. Antonio Imbesi, University of Messina, Piazza Pugliatti 1, I-98122 Messina, Italy*
Email: rosaria.gitto@unime.it

Dedicated to Professor Girolamo Cirrincione

Received 10-29-2021 **Accepted Manuscript** 02-11-2022 **Published on line** 03-02-2022

Abstract

Several studies demonstrated that hyperpigmentation pathologies might be treated by using agents targeting the enzymatic metallo-protein tyrosinase. Therefore, we predicted the development of a series of small molecules able to inhibit diphenolase activity of tyrosinase from *Agaricus bisporus*. The designed compounds were readily synthesized by S-alkylation and the synthesized compounds were tested through biochemical screening, thus providing structure-affinity relationships for this class of 5-(pyridin-4-yl)-3-(alkylsulfanyl)-4*H*-1,2,4-triazol-4-amine derivatives. In addition, docking simulations suggested the binding mode within the catalytic site of the targeted enzyme.

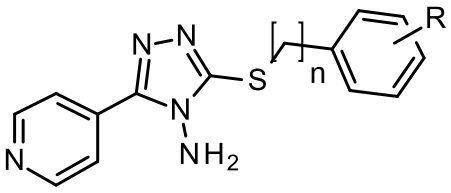

Keywords: S-alkylation, 5-(pyridin-4-yl)-3-(alkylsulfanyl)-4*H*-1,2,4-triazol-4-amines, tyrosinase, melanin.

Introduction

Skin and hair pigmentation varies based on age, body-region and ethnicity, as well as exposure to UV radiation. In terms of pigmentation, a multistep process produces both eumelanin and pheomelanin pigments in melanocytes in physiological conditions.[1] However, an abnormal increase in the number of melanocytes or epidermal melanin biosynthesis is implicated as the cause for several hyperpigmentation diseases, including age spots, freckles, melasma and melanoma.[2, 3]To fight these pathologies a therapeutic approach might consist of the administration of drugs targeting the enzyme tyrosinase (TYR, EC 1.14.18.1) that is involved in the oxidation process of tyrosine amino acid, producing L-DOPA and dopaquinone, which can spontaneously polymerize or combine with peptides to form melanin pigments.[2] Based on the knowledge of this enzymatic pathway, the targeting of tyrosinase inhibitors (TYRIs) has demonstrated efficacy in cosmetic and dermatology applications.[4]

To address this issue, a large number of inhibitors from natural and synthetic sources have been reported in the literature;[1, 5-7] they have generally been identified on the basis of their ability to inhibit tyrosinase from *Agaricus bisporus* (AbTYR), which represents a readily and cheap protocol to preliminarily screen TYRIs.[8, 9] In turn, the best active AbTYR inhibitors were further studied using advanced biological methods, as well as human tyrosinase (hTYR) screening validation through cell-free crude extracts of tyrosinase-expressing cell lines and recombinant hTYR.

Natural and (semi)-synthetic inhibitors of AbTYR include distinct chemical classes of compounds.[9] They might display distinct mode of action as competitive, non-competitive, mixed and uncompetitive inhibitors on the basis of kinetic studies on diphenolase activity of AbTYR.

There are several AbTYR inhibitors from different sources possessing significant differences in chemical structures; the collection of TYRIs includes cinnamic and kojic acid derived compounds (**1, 1a** and **2**), flavonoids, polyphenolic compounds and coumarins, as well as heterocyclic compounds (*e.g.* compound **3**) (see Figure 1).[10-12]

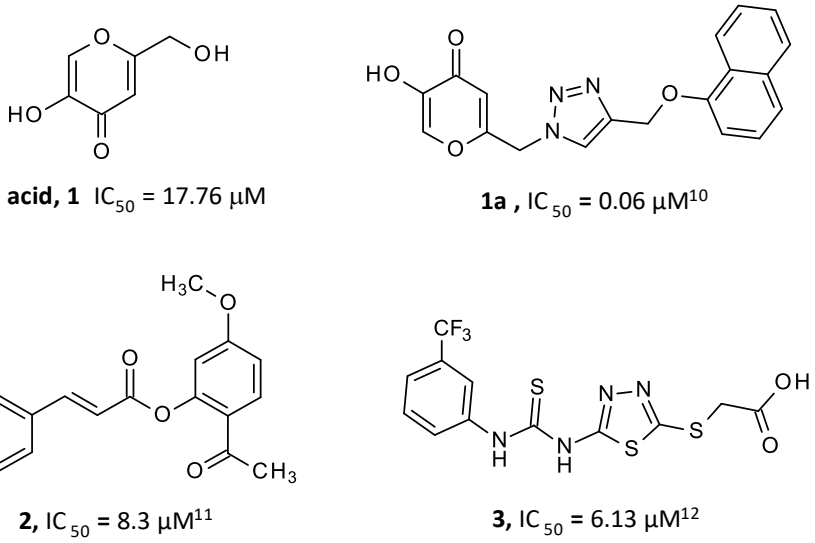

Figure 1. Chemical structures of 5-hydroxy-2-(hydroxymethyl)pyran-4-one (kojic acid, **1**), 5-hydroxy-2-({4-[(naphthalen-1-yloxy)methyl]-1*H*-1,2,3-triazol-1-yl}methyl)-4*H*-pyran-4-one (**1a**), (2-acetyl-5-methoxyphenyl) (*E*)-3-(4-fluorophenyl)prop-2-enoate (**2**) and 2-[(5-{[3-(trifluoromethyl)phenyl]carbamothioylamino}-1,3,4-thiadiazol-2-yl)sulfanyl]acetic acid (**3**) as examples of well-known TYRIs from natural and synthetic sources.

Our previous research on TYRIs resulted in the identification of distinct series of compounds bearing aromatic/heteroaromatic systems linked to a 4-fluorobenzyl moiety, which has been identified as an optimal substituent to exert inhibitory effects toward AbTYR.[13-19] Specifically, we explored the introduction of piperidine or piperazine groups as an amenable linking group to connect the two crucial aromatic fragments interacting within the AbTYR cavity. Docking and crystallographic studies allowed us to obtain structural information about the catalytic site of TYR, thus elucidating the binding mode within this catalytic site for the most active compounds.[15, 16, 19]

Figure 2 displays the chemical structure of the 1-[4-(4-fluorobenzyl)piperazin-1-yl]-(3-chloro-2-nitro-phenyl)methanone (**4**) as one of the most interesting AbTYR inhibitors (IC_{50} value of 0.18 μM) able to exert antimelanogenic effects on B16F10 cells.[18]

To improve our knowledge about the structure-affinity relationships of TYRIs and expand chemical variability, we report herein a further series of compounds inspired by prototype **4**. Specifically, we focused on the three main fragments displayed in Figure 2: i) a substituted aromatic ring (A), ii) a piperazine linker (B), and iii) the 4-fluorobenzyl moiety (C).

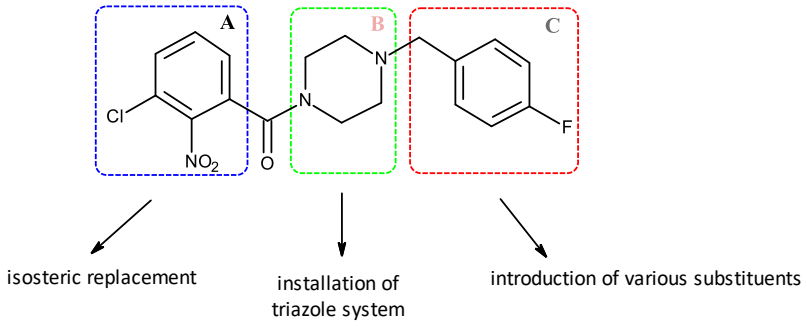

Figure 2. Structural modifications on hit compound **4.**

Firstly, to explore the interactions on the rim of the enzyme active site, the aromatic ring "A" was replaced by isosteric pyridine system. Secondly, we considered the crucial role of the fluorine atom in the above reported derivative **4**; therefore, we looked for further substituents with the same capability to establish profitable contacts in the deeper cavity of TYR and modified portion "C" by decorating the aromatic ring in different positions. Finally, the 1,2,4-triazol-4-amine heterocycle was adopted in place of the piperazine linking group ("B"). The 1,2,4-triazole moiety was selected based on the consideration that it represents a structural building block for many therapeutics, and has been shown to be involved in different biological activities, including anticancer, anticonvulsant antidepressant, antifungal, antibacterial, antiviral activity, and so on.[20-22] The target compounds were synthesized, characterized, and preliminarily screened as potential inhibitors of AbTYR diphenolase activity.

Results and Discussion

To synthesize the designed compounds, we employed the commercially available 4-amino-5–(4-pyridinyl)-4*H*-1,2,4-triazole-3-thiol (**5**), that was combined with an aromatic portion bearing different substituents. To gain additional information about structure-activity relationships (SARs) on AbTYR inhibition, we envisioned that an additional methylene in the linking group might be tolerated in the middle region of the enzymatic cavity.

Scheme 1 depicts the synthetic procedure to obtain the thirteen 5-(pyridin-4-yl)-3-(alkylsulfanyl)-4*H*-1,2,4-triazol-4-amine derivatives **6-18** starting from **5**, via S-alkylation with the suitable aryl halides in alkaline medium at room temperature. All compounds were readily prepared, carefully characterized, and their spectral data (^{1}H-NMR and ^{13}C-NMR) agreed with the proposed structures.

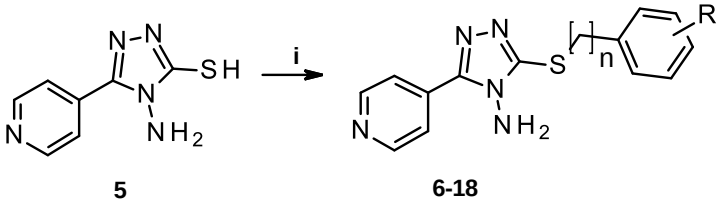

Reagents and conditions
i) $ArCH_2X$ or $Ar(CH_2)_2X$ with X =Cl or Br, NaOH, MeOH, 2.5 h, rt.

Cpd	n	R
6	1	H
7	1	3-F
8	1	4-F
9	1	3-Cl
10	1	4-Cl
11	1	3-CH_3
12	1	4-CH_3
13	1	2,4-F_2
14	1	3,4-F_2
15	1	3,5-$(CH_3)_2$,4-F
16	2	H
17	2	4-F
18	2	4-Cl

Scheme 1. Synthesis of 5-(pyridin-4-yl)-3-(alkylsulfanyl)-4*H*-1,2,4-triazol-4-amine derivatives **6-18.**

All the synthesized compounds were assayed by means of the colorimetric method to test inhibitory effect toward AbTYR. Each experiment was carried out three times and the level of diphenolase activity inhibition was calculated at different concentrations (see experimental section). The results are collected in Table 1, in which we compared the activity with kojic acid (**1**) as well-known reference drug in the determination of inhibitory effects against AbTYR. The biological evaluation revealed that the newly synthesized compounds exhibited a different degree of inhibitory effects in a wide range of IC_{50} values. The SAR investigation involving the phenyl ring, as well as thioalkyl-linking group, is reported below.

The introduction of a fluorine atom at position 4 of the phenyl ring improved the activity, so that compound **8** (IC_{50} 83.61 μM) was more potent that the unsubstituted inactive compound **6**, which stayed inactive up to 350 μM concentration. Notably, the introduction of the fluorine atom at position 3 of the phenyl ring did not affect the activity (IC_{50} > 350 μM, compound **7**). Replacement of the fluorine by a chlorine atom resulted in derivatives **9** and **10** demonstrating weak activity. Interestingly, the introduction of methyl groups resulted in a drop in potency for compounds **11** and **12**. Moreover, disubstituted compounds **13**, **14** and **15** were generally less active than their mono-substituted analogs. Finally, it was found that when an additional methylene bridge was installed, the resulting compound **17** exhibited an improved potency with an IC_{50} value of 24.92 μM, which was more than 3-fold higher than homologue **8**. A similar improvement of inhibitory potency has been found for compounds **16** and **18** bearing a 2-carbon linker from the triazole moiety.

Table 1. Inhibitory effects toward diphenolase activity of AbTYR IC_{50} (μM) measured for designed compounds **6-18** and kojic acid (**1**)

compound	R	n	IC_{50} (μM)[a] ± SD[b]
6	H	1	>350
7	3-F	1	>350
8	4-F	1	83.61 ± 15.65
9	3-Cl	1	248.23 ± 10.63
10	4-Cl	1	222.43 ± 24.02
11	3-CH_3	1	>350
12	4-CH_3	1	>350
13	2,4-F_2	1	69.80 ± 0.52
14	3,4-F_2	1	104.43 ± 4.01
15	3,5-$(CH_3)_2$,4-F	1	>350
16	H	2	255.48 ± 12.30
17	4-F	2	24.92 ± 1.51
18	4-Cl	2	125.55± 4.67
kojic Acid, 1	-	-	17.76 ± 0.18

[a]IC_{50} values represent the concentration that caused 50% enzyme activity loss. All compounds were studied in a set of experiments performed in triplicate. [b]SD standard deviation

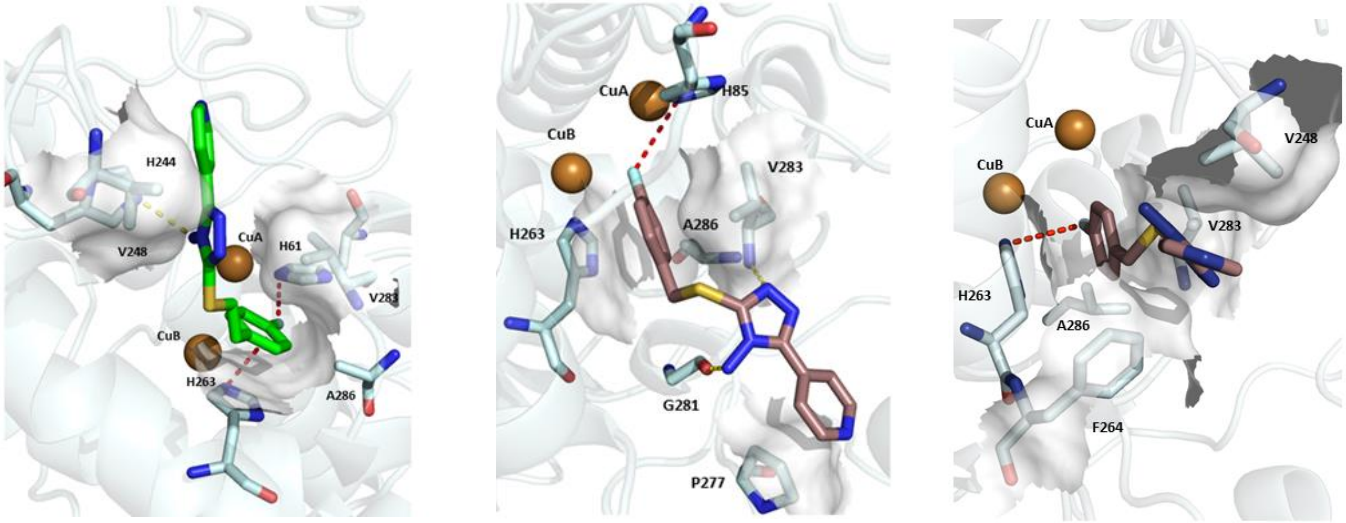

A **B** **C**

Figure 3. Top ranked poses of **17** (Panel A) and **8** (Panel B) and best score pose of the most populated cluster generated for **8** (Panel C), docked into the AbTYR binding site (PDB code 2Y9X)[24] via GOLD software.[23] Compounds **17** and **8** are represented as green and brown sticks, respectively. The amino acid residues of the binding site are represented by cyan sticks, while copper ions are represented as orange spheres. Halogen bonds are highlighted as red dashed lines while H-bonds are represented as yellow dashed lines. White surfaces surround instead residues involved in hydrophobic or π- π interactions. The image was created by using PyMOL software (www.pymol.org)

To hypothesize the binding mode for this newer series of inhibitors, docking studies were performed by using Gold software[23] employing the crystal structure of TyM from *A. bisporus* (PDB 2Y9X).[24] In particular, our interest was to predict the binding interaction for the most promising compound **17** (IC_{50} of 24.92 μM); moreover, we analyzed its binding orientation in comparison with analog compound **8**, which demonstrated less capability to bind catalytic site of AbTYR (IC_{50} of 83.61 μM).

Docking results for compound **17** identified the top ranked pose; the best one of the most populated cluster overlapped in only one pose (Figure 3A) showing a fitness score value of 68.05. Regarding compound **8**, GOLD software identified two plausible binding-modes referred to (i) the highest scored pose (fitness score 65.09, Figure 3B) and (ii) to the best pose of the most abundant cluster (fitness score 56.76, Figure 3C). The different fitness score values calculated for compounds **17** and **8** were consistent with their different degree of inhibitory effects measured against AbTYR enzymatic activity respectively (IC_{50} = 24.92 μM vs IC_{50}=83.61 μM).

Based on the analysis made by Discovery Studio Visualizer, we found that both inhibitors were able to establish productive contacts in the region located near the copper ions, so that no relevant differences in the number of interactions was found. In fact, the *para*-fluorobenzyl moiety were found to be oriented toward the copper ions as described for the hit compound **4**.[18] The models of interaction revealed more appreciable differences in the contacts made by the pyridine ring and 1,2,4-triazole core. The pyridine ring of compound **17** reached a hydrophobic surface on the rim of the active site, establishing π – π interactions with His244. Furthermore, the binding orientation of derivative **17** ws also stabilized through a hydrogen bond interaction between the amine NH_2 group of 1,2,4-triazole moiety and His244. The lack of the above-mentioned interactions in the poses evaluated for compound **8** might explain its lower potency to inhibit AbTYR. This could be addressed by the additional methylene group incorporated into the S-linking fragment of compound **17**, which could permit the occupancy of a wider portion of the druggable space, apart from enhancing the molecule flexibility (see Figure 3A).

To evaluate the stability of the predicted binding modes, we also performed an MM-GBSA free energy calculation of the poses evaluated through docking analysis (see Table 2). As confirmation of the best activity of **17**, its pose displayed a ΔG binding affinity considerably higher compared to that of compound **8**.

Table 2. Binding-free energy values (kcal/mol) obtained by Prime MM–GBSA[25] for the analyzed docking poses of derivatives **17** and **8**

Compound	ΔG_{bind} (kcal/mol)
Top ranked poses of 17	- 45.82
Top ranked poses of 8	-12.94
Best score poses of the most populated cluster generated for 8	- 32.93

Conclusions

In conclusion, guided by previously SAR information, a small series of thirteen 5-(pyridin-4-yl)-3-(alkylsulfanyl)-4*H*-1,2,4-triazol-4-amine-based compounds were studied as inhibitors of AbTYR. Compound **17** proved to be an active inhibitor at micromolar concentrations. The binding mode was suggested by means of docking simulation; the ChemPLP score and MM-GBSA binding energy value calculated, and the results were in good agreement with the biological results. Taken together, these data provide additional information for further investigations of TYRIs from synthetic sources.

Experimental Section

General. All reagents were used without further purification and bought from common commercial suppliers. Melting points were determined on a Buchi B-545 apparatus (BUCHI Labortechnik AG Flawil, Switzerland). By combustion analysis (C, H, N), carried out on a Carlo Erba Model 1106-Elemental Analyser, we determined the purity of synthesised compounds; the results confirmed a ± 95% purity. Merck Silica Gel 60 F254 plates were used for analytical TLC (Merck KGaA, Darmstadt, Germany). For detection, iodine vapour and UV light (254 nm) were used. ^{1}H and ^{13}C NMR spectra were recorded in DMSO-d_6 with a Varian Gemini 500 spectrometer (Varian Inc. Palo Alto, California USA); chemical shifts (δ) and coupling constants (*J*) are given in ppm and hertz, respectively. For each designed compound, we evaluated the adherence to the Lipinski's rule and the absence of PAINS in silico by using SwissADME (http://www.swissadme.ch) (see Supplementary Material). For compounds **6-8**, **10-12** and **16** registered CAS numbers have been already assigned and are available at https://www.cas.org. Their synthetic pathway, chemical properties and structural characterization agree with what has already been reported in the literature.[26, 27]

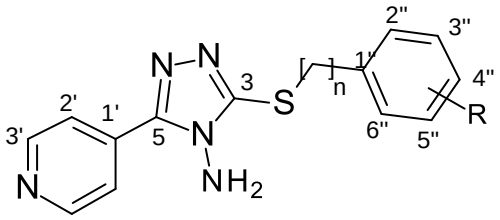

General procedure for the synthesis of 5-(pyridin-4-yl)-3-(alkylsulfanyl)-4*H*-1,2,4-triazol-4-amine derivatives 9, 13-15, and 17-18. The 4-amino-5–(4-pyridinyl)-4*H*-1,2,4-triazole-3-thiol (**5**) (200 mg, 1.03 mmol) and NaOH (41 mg, 1.02 mmol) were dissolved in MeOH (8 mL); after complete dissolution, the suitable alkyl halide derivative (1.03 mmol) was added dropwise. We generally employed alkyl bromide derivatives to prepare designed compounds, except for desired compound **9** for which we used the suitable alkyl chloride derivative. The reaction mixture was stirred for 2.5 hours at room temperature. Upon completion of the reaction, the solvent was removed under reduced pressure and the solid residue was re-crystalized from diethyl ether/ethanol, providing the pure final pyridyl-triazole derivatives as a powder. The registered CAS number for compound **9** has been already assigned and is available at https://www.cas.org; however, its synthetic procedure, chemical and structural characterization are not available in literature.

3-[(3-Chlorobenzyl)sulfanyl]-5-(pyridin-4-yl)-4*H*-1,2,4-triazol-4-amine (9). CAS number: 676335-85-6. Yield 88%. Off-white solid. mp 183-185°C. ^{1}H NMR (500 MHz, DMSO- d_6): δ_H 4.46 (2H, s, CH_2); 6.24 (2H, bs, NH_2); 7.31-7.37 (2H, m, ArH, H-5" and H-6"); 7.42-7.44 (1H, m, ArH, H-4"); 7.53 (1H, m, ArH, H-2"); 7.98-8.00 (2H, dd, *J* 4.5, 1.7 Hz, pyridine, H-2" and H-6"); 8.72-8.73 (2H, dd, *J* 4.5, 1.6 Hz, pyridine, H-3" and H-5"). ^{13}C NMR (126 MHz, DMSO- d_6): δ_C 33.9 (CH_2); 121.3 (C-2' and C-6', pyridine); 127.3 (C-2''); 127.8 (C-4''); 128.8 and 130.2 (C-5'' and C-6"); 132.8 (C-3''); 133.9 (C-1', pyridine); 140.3 (C-1"); 150.1 (C-3' and C-5', pyridine); 152.1 and 154.3 (C-3 and C-5). Anal. Calcd for $C_{14}H_{12}ClN_5S$ (317.79): C, 52.91; H, 3.81; N, 22.04. Found: C, 52.86; H, 3.80; N, 21.97.

3-[(2,4-Difluorobenzyl)sulfanyl]-5-(pyridin-4-yl)-4*H*-1,2,4-triazol-4-amine (13). Yield 100%. Yellowish solid. mp 163-165°C. ^{1}H NMR (500 MHz, DMSO- d_6): δ_H 4.46 (2H, s, CH_2); 6.30 (2H, s, NH_2); 7.03-7.06 (1H, m, ArH, H-2"); 7.23-7.27 (1H, m, ArH, H-6"); 7.57-7.62 (1H, m, ArH, H-5"); 8.05 (2H, d, *J* 5.9 Hz, pyridine, H-2" and H-6"); 8.74 (2H, d, *J* 5.9 Hz, pyridine, H-3" and H-5"). ^{13}C NMR (126 MHz, DMSO-d_6): δ_C 28.5 (CH_2); 104.3 (C-3"); 111.8 (C-5"); 118.9 (C-1"); 121.9 and 121.9 (C-2' and C-6', pyridine); 132.9(C-6"); 134.7 (C-1', pyridine); 150.1 and 150.2 (C-3'

and C-5', pyridine); 152.5 and 154.5 (C-3 and C-5); 161.5 (C-2" and C2", *J*= 240 Hz). Anal. Calcd for $C_{14}H_{11}F_2N_5S$ (319.33): C, 52.66; H, 3.47; N, 21.93. Found: C, 52.88; H, 3.20; N, 22.10.

3-[(3,4-Difluorobenzyl)sulfanyl]-5-(pyridin-4-yl)-4*H*-1,2,4-triazol-4-amine (14). Yield 100%. White solid. mp 151-153°C. ^{1}H NMR (500 MHz, DMSO-d_6): δ_H 4.46 (2H, s, CH_2); 6.31 (2H, s, NH_2); 7.32-7.40 (2H, m, ArH, H-2" and H-5"); 7.53-7.57 (1H, m, ArH, H-6"); 8.02 (2H, d, *J* 5.8 Hz, pyridine, H-2" and H-6"); 8.72 (2H, d, *J* 5.8 Hz, pyridine, H-3" and H-5"). ^{13}C NMR (126 MHz, DMSO-d_6): δ_C 33.7; 117.3 and 118.0 (C-2" and C-5"); 121.3 (C-2' and C-6', pyridine); 126.0 (C-6"); 133.9 (C-1', pyridine); 135.7 (C-1"); 147.7 and 149.8 (C-3" and C-4"); 150.1 (C-3' and C-5', pyridine); 152.1 and 154.2 (C-3 and C-5). Anal. Calcd for $C_{14}H_{11}F_2N_5S$ (319.33): C, 52.66; H, 3.47; N, 21.93. Found: C, 52.72; H, 3.40; N, 21.80.

3-[(4-Fluoro-3,5-dimethylbenzyl)sulfanyl]-5-(pyridin-4-yl)-4*H*-1,2,4-triazol-4-amine (15). Yield 100%. Yellow solid. mp 175-177°C. ^{1}H NMR (500 MHz, DMSO-d_6): δ_H 2.18 (6H, s, $2CH_3$); 4.37 (2H, s, CH_2); 6.25 (2H, s, NH_2); 7.16 (2H, d, *J* 7.09 Hz, ArH, H-2" and H-6"); 8.01 (2H, d, *J* 6.13 Hz, pyridine, H-2" and H-6"); 8.72 (2H, d, *J* 6.13 Hz, pyridine, H-3" and H-5"). ^{13}C NMR (126 MHz, DMSO-d_6): δ_C 14.2 (CH_3); 14.3 (CH_3); 34.5 (CH_2); 121.3 and 121.5 (C-2' and C-6', pyridine); 123.7 and 123.8 (C-3" and C-5"); 129.6 and 129.8 (C-2" and C-6"); 132.5 (C-1"); 133.9 (C-1', pyridine); 150.0 and 150.2 (C-3' and C-5', pyridine); 152.0 and 154.5 (C-3 and C-5); 158.8 (C-4", d, $J_{C\text{-}F}$ 242 Hz). Anal. Calcd for $C_{16}H_{16}FN_5S$ (329.39): C, 58.34; H, 4.90; N, 21.26. Found: C, 58.39; H, 4.82; N, 21.31.

3-[(4-Fluorophenethyl)sulfanyl]-5-(pyridin-4-yl)-4*H*-1,2,4-triazol-4-amine (17). Yield 84%. Yellowish solid. mp 128-130°C. ^{1}H NMR (500 MHz, DMSO-d_6): δ_H 3.04 (2H, t, *J* 7.3 Hz, CH_2); 3.44 (2H, t, *J* 7.3 Hz, CH_2); 6.24 (2H, s, NH_2); 7.11-7.14 (2H, m, ArH, H-3" and H-5"); 7.32-7.35 (2H, m, ArH, H-3" and H-5"); 8.02 (2H, d, *J* 4.6 Hz, pyridine, H-2" and H-6"); 8.72 (2H, d, *J* 4.6 Hz, pyridine, H-3" and H-5"). ^{13}C NMR (126 MHz, DMSO-d_6): δ_C 32.4 (CH_2); 34.2 (CH_2); 115.1 (C-3" and C-5"); 121.3 and 121.4 (C-2' and C-6', pyridine); 130.3 and 130.5 (C-2" and C-6"); 134.0 (C-1', pyridine); 135.9 (C-1"); 149.9 and 150.1 (C-3' and C-5', pyridine); 151.9 and 154.9 (C-3 and C-5); 161.4 (C-4", d, $J_{C\text{-}F}$ 241. Hz). Anal. Calcd for $C_{15}H_{14}FN_5S$ (315.36): C, 57.13; H, 4.47; N, 22.21. Found: C, 56.82; H, 4.75; N, 22.56.

3-[(4-Chlorophenethyl)sulfanyl]-5-(pyridin-4-yl)-4*H*-1,2,4-triazol-4-amine (18). Yield 100%. Off-white solid. mp 162-164°C. ^{1}H NMR (500 MHz, DMSO-d_6): δ_H 3.04 (2H, t, *J* 7.3 Hz, CH_2) 3.43 (2H, t, *J* 7.1 Hz, CH_2); 6.24 (2H, s, NH_2); 7.32-7.37 (4H, m, ArH); 8.01 (2H, d, *J* 4.5 Hz, pyridine, H-2" and H-6"); 8.72 (2H, d, *J* 4.5 Hz, pyridine, H-3" and H-5"). ^{13}C NMR (126 MHz, DMSO-d_6): δ_C 32.2 (CH_2); 34.3 (CH_2); 121.3 and 121.4 (C-2' and C-6', pyridine); 128.2 and 128.4 (C-3" and C-5"); 130.4 and 130.7 (C-2" and C-6"); 131.0 (C-4"); 133.9 (C-1', pyridine); 138.8 (C-1"); 149.9 and 150.2 (C-3' and C-5', pyridine); 151.9 and 154.8 (C-3 and C-5). Anal. Calcd for $C_{15}H_{14}ClN_5S$ (331.82): C, 54.30; H, 4.25; N, 21.11. Found: C, 54.58; H, 4.22; N, 21.33.

Mushroom tyrosinase inhibition assay

Tyrosinase inhibition was assayed according to the method of Masamoto,[28] with minor modifications.[29] Briefly, aliquots (0.05 mL) of sample at various concentrations (5-350 μM) were mixed with 0.5 mL of L-DOPA solution (1.25 mM), 0.9 mL of sodium acetate buffer solution (0.05 M, pH 6.8) and preincubated at 25°C for 10 min. Then 0.05 mL of an aqueous solution of mushroom tyrosinase (333 U/mL) was added last to the mixture. The linear increase in absorbance (Abs) at 475 nm was measured in the reaction mixture up to 5 minutes. The inhibitory activity of samples is expressed as inhibition percentage. The concentrations leading to 50% activity loss (IC_{50}) were also calculated by interpolation of the dose-response curves. Kojic acid [5-hydroxy-2-(hydroxymethyl)-4*H*-pyran-4-one, **1**], a fungal secondary metabolite used as skin whitening agent, was employed as a positive standard (8-35 μM).

Molecular Docking on AbTYR

The crystal structure of tyrosinase from the mushroom *Agaricus bisporus* (AbTYR) in complex with the inhibitor tropolone was retrieved from the RCSB Protein Data Bank (PDB code 2Y9X).[24] The ligand and water molecules

were discarded, and the hydrogen atoms were added to the protein by Discovery Studio 2020 (https://www.3ds.com). The ligands were prepared using a protocol implemented in VEGA suite 3.2.1 which comprehended: calculation of charges and potential using SP4 forcefields and Gasteiger as charge calculation method; a first minimization of 1000 steps, a conformational search using systematic method; a second minimization of 1000 steps. All the other settings were left as default.[30] The prepared ligands were docked into the corresponding protein by means of Gold software V 2020.2.0, keeping the protein rigid. The region of interest used by the Gold program was defined in order to contain the residues within 10 Å from the original position of the ligand in the X-ray structure. Atom types for the ligands and for the protein were also set by GOLD. ChemPLP was used as scoring function. The standard default settings were used in all calculations and the ligands were submitted to 100 genetic algorithm runs. The "allow early termination" command was deactivated. Results differing by less than 0.75 Å in ligand-all atom RMSD were clustered together. The highest score pose as well as the best score pose of the most populated cluster were then selected for analysis and submitted to MM-GBSA binding energy calculation on Prime using the default settings.[25] Visualization and interaction analysis of the docking results were carried out by means of Discovery Studio 2020.

Acknowledgements

This work was supported by the MIUR – "Finanziamento delle Attività Base di Ricerca" FFABR UNIME funding.

Supplementary Material

^{1}H and ^{13}C NMR spectra, ADME profile, smiles strings

References

1. Roulier, B.;Peres, B.;Haudecoeur, R. *J Med Chem* **2020**, *63*, 13428-13443. https://doi.org/10.1021/acs.jmedchem.0c00994
2. Pillaiyar, T.;Namasivayam, V.;Manickam, M.;Jung, S. H. *J Med Chem* **2018**, *61*, 7395-7418. https://doi.org/10.1021/acs.jmedchem.7b00967
3. Sorg, H.;Tilkorn, D. J.;Hager, S.;Hauser, J.; Mirastschijski, U. *Eur Surg Res* **2017**, *58*, 81-94. https://doi.org/10.1159/000454919
4. Pillaiyar, T.;Manickam, M.;Namasivayam, V. *J Enzyme Inhib Med Chem* **2017**, *32*, 403-425. https://doi.org/10.1080/14756366.2016.1256882
5. Bonesi, M.;Xiao, J.;Tundis, R.;Aiello, F.;Sicari, V.;Loizzo, M. R. *Curr Med Chem* **2019**, *26*, 3279-3299. https://doi.org/10.2174/0929867325666180522091311
6. Orhan, I. E.;Deniz, F. S. S. *Curr Pharm Biotechnol* **2021**, *22*, 1412-1423. https://doi.org/10.2174/1386207323666201211102233
7. Yuan, Y.;Jin, W.;Nazir, Y.;Fercher, C.;Blaskovich, M. A. T.;Cooper, M. A.;Barnard, R. T.;Ziora, Z. M. *Eur J Med Chem* **2020**, *187*, 111892. https://doi.org/10.1016/j.ejmech.2019.111892
8. Peng, Z.;Wang, G.;Zeng, Q. H.;Li, Y.;Liu, H.;Wang, J. J.;Zhao, Y. *Crit Rev Food Sci Nutr* **2021**, 1-42.

https://doi.org/10.1080/10408398.2021.1871724
9. Zolghadri, S.;Bahrami, A.;Hassan Khan, M. T.;Munoz-Munoz, J.;Garcia-Molina, F.;Garcia-Canovas, F.;Saboury, A. A. *J Enzyme Inhib Med Chem* **2019**, *34*, 279-309. https://doi.org/10.1080/14756366.2018.1545767
10. Ashooriha, M.;Khoshneviszadeh, M.;Moradi, S. E.;Rafiei, A.;Kardan, M.;Emami, S. *Bioorg Chem* **2019**, *82*, 414-422. https://doi.org/10.1016/j.bioorg.2018.10.069
11. Sheng, Z.;Ge, S.;Xu, X.;Zhang, Y.;Wu, P.;Zhang, K.;Li, C.;Zhao, D.;Tang, X. *MedChemComm* **2018**, *9*, 853-861 https://doi.org/10.1039/C8MD00099A
12. Liu, P.;Shu, C.;Liu, L.;Huang, Q.;Peng, Y. *Bioorg Med Chem* **2016**, *24*, 1866-1871. https://doi.org/10.1016/j.bmc.2016.03.013
13. De Luca, L.;Germano, M. P.;Fais, A.;Pintus, F.;Buemi, M. R.;Vittorio, S.;Mirabile, S.;Rapisarda, A.;Gitto, R. *Bioorg Med Chem* **2020**, *28*, 115497.1.Roulier, B.;Peres, B.;Haudecoeur, R. J Med Chem 2020, 63, 13428-13443. https://doi.org/10.1021/acs.jmedchem.0c00994
14. Ferro, S.;Certo, G.;De Luca, L.;Germanò, M. P.;Rapisarda, A.;Gitto, R. *J Enzyme Inhib Med Chem* **2016**, *31*, 398-403 http://doi.org/10.3109/14756366.2015.1029470
15. Ferro, S.;De Luca, L.;Germanò, M. P.;Buemi, M. R.;Ielo, L.;Certo, G.;Kanteev, M.;Fishman, A.;Rapisarda, A.;Gitto, R. *Eur J Med Chem* **2017**, *125*, 992-1001. https://doi.org/10.1016/j.ejmech.2016.10.030
16. Ferro, S.;Deri, B.;Germanò, M. P.;Gitto, R.;Ielo, L.;Buemi, M. R.;Certo, G.;Vittorio, S.;Rapisarda, A.;Pazy, Y.;Fishman, A.;De Luca, L. *J Med Chem* **2018**, *61*, 3908-3917. https://doi.org/10.1021/acs.jmedchem.7b01745
17. Ielo, L.;Deri, B.;Germano, M. P.;Vittorio, S.;Mirabile, S.;Gitto, R.;Rapisarda, A.;Ronsisvalle, S.;Floris, S.;Pazy, Y.;Fais, A.;Fishman, A.;De Luca, L. *Eur J Med Chem* **2019**, *178*, 380-389. https://doi.org/10.1016/j.ejmech.2019.06.019
18. Mirabile, S.;Vittorio, S.;Paola Germano, M.;Adornato, I.;Ielo, L.;Rapisarda, A.;Gitto, R.;Pintus, F.;Fais, A.;De Luca, L. *ChemMedChem* **2021**, *16*, 3083-3093. https://doi.org/10.1002/cmdc.202100396
19. Vittorio, S.;Ielo, L.;Mirabile, S.;Gitto, R.;Fais, A.;Floris, S.;Rapisarda, A.;Germanò, M. P.;De Luca, L. *ChemMedChem* **2020**, *15*, 1757-1764. https://doi.org/10.1002/cmdc.202000125
20. Jain, A.;Piplani, P. *Mini Rev Med Chem* **2019**, *19*, 1298-1368. https://doi.org/10.2174/1389557519666190312162601
21. Kharb, R.;Sharma, P. C.;Yar, M. S. *J Enzyme Inhib Med Chem* **2011**, *26*, 1-21. https://doi.org/10.3109/14756360903524304
22. Kucukguzel, S. G.;Senkardes, S. *Eur J Med Chem* **2015**, *97*, 786-815. https://doi.org/10.1016/j.ejmech.2014.11.059
23. Jones, G.;Willett, P.;Glen, R. C.;Leach, A. R.;Taylor, R. *J Mol Biol* **1997**, *267*, 727-748. https://doi.org/10.1006/jmbi.1996.0897
24. Ismaya, W. T.;Rozeboom, H. J.;Weijn, A.;Mes, J. J.;Fusetti, F.;Wichers, H. J.;Dijkstra, B. W. *Biochemistry* **2011**, *50*, 5477-5486. https://doi.org/10.1021/bi200395t

25. Jacobson, M. P.;Pincus, D. L.;Rapp, C. S.;Day, T. J.;Honig, B.;Shaw, D. E.;Friesner, R. A. *Proteins* **2004**, *55*, 351-367. https://doi.org/10.1002/prot.10613
26. Kolodina, A. A.;Gaponenko, N. I.;Lesin, A. V. *Russ Chem Bull* **2008**, *57*, 1273-1276. https://doi.org/10.1007/s11172-008-0164-y
27. Vittorio, S.;Adornato, I.;Gitto, R.;Pena-Diaz, S.;Ventura, S.;De Luca, L. *J Enzyme Inhib Med Chem* **2020**, *35*, 1727-1735. https://doi.org/10.1080/14756366.2020.1816999
28. Masamoto, Y.;Ando, H.;Murata, Y.;Shimoishi, Y.;Tada, M.;Takahata, K. *Biosci Biotechnol Biochem* **2003**, *67*, 631-634. https://doi.org/10.1271/bbb.67.631
29. Smeriglio, A.;D'Angelo, V.;Denaro, M.;Trombetta, D.;Raimondo, F. M.;Germano, M. P. *Chem Biodivers* **2019**, *16*, e1900314. https://doi.org/10.1002/cbdv.201900314
30. Pedretti, A.;Mazzolari, A.;Gervasoni, S.;Fumagalli, L.;Vistoli, G. *Bioinformatics* **2021**, *37*, 1174-1175. https://doi.org/10.1093/bioinformatics/btaa774